3-3-1993

ROBUST CALIBRATION METHODS FOR ONEPORT ACOUSTIC NETWORK ANALYZERS WITH MULTIPLE STANDARD REFLECTORS

R.F.M. (Rob) van den Brink and C.M. (Kees) de Blok

PTT Research,
PO BOX 421,
2260 AK Leidschendam,
The Netherlands.
telefax +31.70.3326477

ABSTRACT

An improved mathematical method is here proposed to extract the de-embedding parameters of one-port Acoustic Network Analyzers, equipped with full error correction. Acoustic Network Analyzers are used for calibrated measurements of acoustic reflection, impedance and admittance of objects in regular tubes. The improved calibration method is primarily based on redundancy by using a large number of standard reflectors, and secondly on the spreading of errors in a balanced way. This has made the calibration method robust and insensitive to small errors, as compared to a simple three-point calibration.

The applicability of the instrument has been improved by using different calibration methods for reflection, impedance and admittance measurements. Because absolute impedance values range from zero to infinity, methods are proposed to handle extreme values in case of impedance or admittance de-embedding.

Iterative calculation methods are avoided by linearization of the calibration equations. As a result, the de-embedding parameters are resolved in closed mathematical form. The linearization has been achieved by error weighting, at the cost of a small degradation in accuracy balance.
Therefore, various accuracy aspects are analyzed in detail. First, the error weighting and the influence of error weighting on error spreading is calculated. Next, the influence of the standard reflector accuracy on the overall de-embedding accuracy is evaluated. Finally, the accuracy analysis has resulted in recommendations for different calibration methods associated with different measurement ranges, in case of impedance or admittance de-embedding.

The proposed methods are demonstrated experimentally and compared with a simple three-point calibration.

0. INTRODUCTION

In many practical problems, acoustic properties such as absorption and reflection of porous material, resonating effects in loudspeaker cabinets or the radiation impedance of acoustic sources have to be determined by measurement. In a well-defined measurement setup, the measurement object is embedded in a closed acoustic system and linked to an acoustic driver via regular tubes. If the measuring object has only one connection with the measuring instrument, it is called a one-port.
A classic and wide-used method for reflection measurement is based on the detection of successive minima and maxima of the standing wave pattern in a

tube, terminated with the measuring object (one-port). However, this technique is time consuming since the traversing mechanism is usually operated manually. Recently, a one-port Acoustic Network Analyzer, with direct reading capabilities, has been developed [1] for reflection measurements on guided acoustic waves in regular tubes. Figure 1 shows two examples of one-port measurements with an acoustic Network Analyzer.

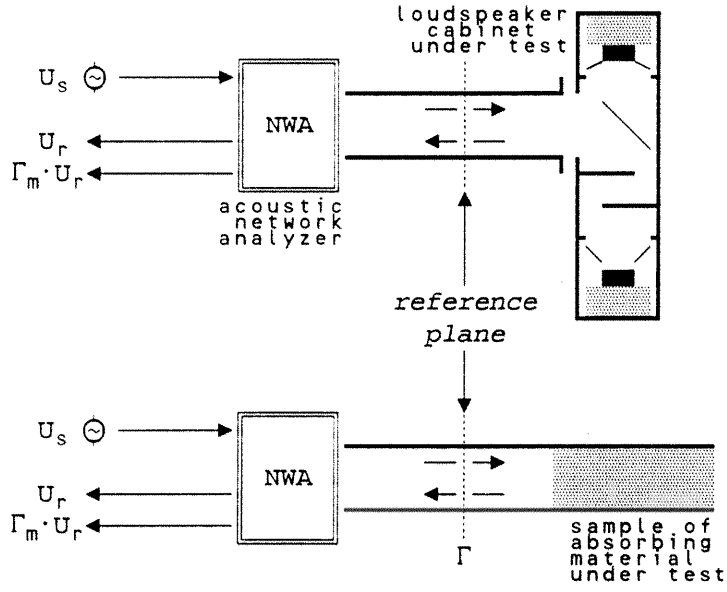


Fig 1 *Two examples of reflection measurements on acoustic objects, using a Network Analyzer. An electrical stimulus signal U_s causes an acoustic wave, and the reflected wave causes the Network Analyzer to generate two electrical signals: U_r and $\Gamma_m \cdot U_r$. The measurement target is the complex reflection coefficient Γ, observed through a well defined reference plane, which is closely related to the magnitude ratio $|\Gamma_m|$ and phase difference $\angle\Gamma_m$ between the two electrical response signals.*

As a consequence of frequency dependent effects in the Network Analyzer and other linear errors, the measured reflection Γ_m will not correspond with the actual reflection Γ, observed through a well-defined reference plane. A complete cancellation of all these linear errors by mechanical improvement is essentially impossible [2], because this requires a Network Analyzer with infinite small dimensions.
A superior improvement method above mechanical improvement is demonstrated in ref. [2] and uses mathematical techniques to correct for all these linear measurement errors. The mathematical error correction is based on a linear error model of the measurement setup which fully characterizes the one-port Network Analyzer with three [2] error correcting parameters.

An essential procedure for mathematical error correction is the extraction of the three error-correcting parameters, which is called calibration. During calibration, various measured reflection values Γ_m are compared with the associated actual reflection values Γ obtained from measurements on well-defined standard reflectors. Based on the difference between the measured values and the actual reflections, the error parameters are reconstructed.

Convenient reflectors for usage as standard reflector are: (offset) Covers, (offset) Opens and ideal Absorbers. An offset Cover or Open is a tube that is covered or left open at its end, at a well defined position. The offset is defined as the distance between the chosen location of the reference

plane and the tube end. An Absorber is something like an open tube, filled with absorbing material.
Covers with zero offset have a reflection coefficient of $\Gamma=1$, which makes them attractive for calibration purposes. Opens with zero offset have a reflection coefficient of $\Gamma\approx-1$, due to minor radiation effects, which makes them second best as choice for standard reflector. Ideal Absorbers have zero reflection by definition, but are difficult to realize with high accuracy.

In ref. [2], a simple calibration method is described, based on measurements of exactly three standard reflectors. Although that calibration method is capable of a drastic improvement of the measurement accuracy and measurement bandwidth, its final accuracy is sensitive to small errors during the calibration.
These calibration errors are caused by distortion, quantization, drift, noise and hum in the Network Analyzer [2], and by the limited accuracy of the standard reflectors. For instance, in case an offset Cover is used as standard reflector, the inaccuracy in sound velocity forms one of the principal accuracy limitations, because it varies with ambient temperature and humidity.

In this article, we propose an improved calibration method, in which the calibration errors are reduced by appropriate averaging techniques. The method uses the raw measurements on more than three standard reflectors and resolves the overdetermined calibration equations in a least-squares sense. As a result, the errors are symmetrically spread out over all measurements and individual errors do not deteriorate the overall accuracy.

1. DE-EMBEDDING EQUATIONS

Figure 2 shows an appropriate linear error model of a one-port Acoustic Network Analyzer for mathematical error correction of linear instrument errors. It is basically an ideal Network Analyzer cascaded with a virtual acoustic two-port. As was demonstrated in ref. [2], all linear instrument errors can be combined and thought of as concentrated in this virtual acoustic two-port.
Although the chosen two-port representation is irrelevant, we will confine ourselves to a normalized representation with scattering parameters [2],[3].

The advantage of the linear error model in figure 2 is that the scattering parameters of the virtual two-port facilitate the derivation of a mathematical relationship between actual and measured reflection coefficients. The mathematical reconstruction of the actual reflection from the measured reflection is based on one of these relationships.
Another advantage is the possibility to position the reference plane on an arbitrary location. In practical situations, the object of measurement is linked with the analyzer by an acoustic wave guide, and this tube affects the measurement result. The use of mathematical error correction facilitates the positioning of the reference plane at any location in this wave guide.

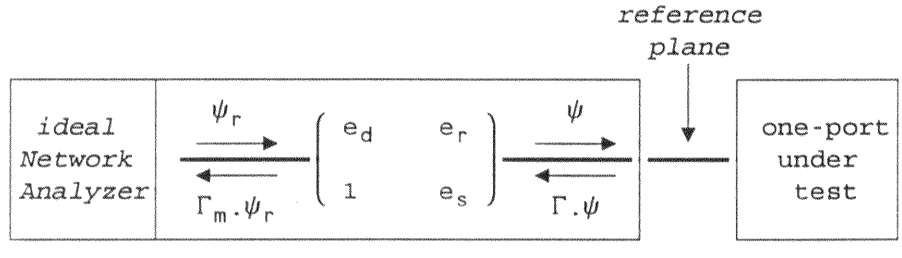


Fig 2 Full linear error model for a one-port Acoustic Network

Analyzer, with normalized error correcting scattering parameters.

The actual reflection Γ through the reference plane is embedded in the wave guide between the virtual error two-port and the object of measurement. When all three scattering parameters $[e_d, e_r, e_s]$ are known, then the actual value of Γ can be reconstructed from the measured value Γ_m.

The reconstruction of a measurement target from raw measurements, such as reflection, impedance or admittance, is called *de-embedding*, and the required set of parameters, such as $[e_d, e_r, e_s]$, are called *de-embedding parameters*, or *error-correcting parameters*.
The measurement and extraction procedure of the de-embedding parameters from measurements on well defined reflectors, is called *calibration*.

In ref. [2] the derivation of a de-embedding equation is described, but this was limited to reflection de-embedding. Although the Acoustic Network Analyzer is primarily intended for reflection de-embedding, a simple transformation of reflection into acoustic impedance Z or acoustic admittance Y will extend the applicability of the instrument. Figure 3 tabulates the de-embedding equations for reflection, impedance and admittance for various sets of de-embedding parameters.

mutual relation	$[e_d, e_r, e_s]$	$[e_d, \Delta_E, e_s]$
$\Gamma = \frac{Z - \mathbb{Z}_0}{Z + \mathbb{Z}_0}$	$= \frac{(e_d - \Gamma_m)}{e_s \cdot (e_d - \Gamma_m) - e_r}$	$= \frac{e_d - \Gamma_m}{\Delta_E - e_s \cdot \Gamma_m}$
$Z/\mathbb{Z}_0 = \frac{1 + \Gamma}{1 - \Gamma}$	$= \frac{(e_s+1) \cdot (e_d - \Gamma_m) - e_r}{(e_s-1) \cdot (e_d - \Gamma_m) - e_r}$	$= \frac{(\Delta_E+e_d) - (e_s+1) \cdot \Gamma_m}{(\Delta_E-e_d) - (e_s-1) \cdot \Gamma_m}$
$Y \cdot \mathbb{Z}_0 = \frac{1 - \Gamma}{1 + \Gamma}$	$= \frac{(e_s-1) \cdot (e_d - \Gamma_m) - e_r}{(e_s+1) \cdot (e_d - \Gamma_m) - e_r}$	$= \frac{(\Delta_E-e_d) - (e_s-1) \cdot \Gamma_m}{(\Delta_E+e_d) - (e_s+1) \cdot \Gamma_m}$

Fig 3 *Basic de-embedding equations of the actual reflection (Γ), impedance (Z) or admittance (Y) from the measured reflection Γ_m, with $[e_d, e_r, e_s]$ or $[e_d, \Delta_E, e_s]$ as de-embedding parameters.*
e_d = *directivity parameter*
e_s = *source match parameter*
e_r = *reflection tracking parameter*
Δ_E = *matrix determinant* $(e_d e_s - e_r)$

2. ROBUST CALIBRATION WITH MULTIPLE STANDARDS

The calibration for the reconstruction of three de-embedding parameters, can be performed in various ways but always requires at least three independent measurements. One of these methods was described in detail in ref. [2]. Although the reflection of many Covers, Opens and Absorbers were measured, the described method used only three Covers per frequency. The lack of redundancy has prevented this calibration method from being robust, and causes the result to be sensitive to small errors.

The overall accuracy of the calibration is limited by the accuracy of the standard reflector models, and by distortion, drift, noise and hum in the Network Analyzer. For example, a small error in the measurement of an offset distance will cause an error in the reflection phase which increases with the frequency. A robust solution to this problem, that reduces the sensiti-

vity to small calibration errors, is the use of a large number of standard reflectors and an appropriate averaging over all these measurements.

In the case of three standard reflectors, the reconstructed values of the error correcting parameters are unique, and independent of the used calculation method. When these values are used for reflection de-embedding, then the error is forced to zero for these three reflectors, at the cost of decreasing the de-embedding accuracy for other reflectors.
In an overdetermined calibration, the concept *"best estimation"* is closely related to the measurement target: Γ, Z or Y. All calibration errors are then spread out over all calibration samples in a way that minimizes the average de-embedding error.

2.1 NEAR OPTIMAL CALIBRATION

Assume that T represents the actual value of measurement targets such as reflection, impedance or admittance, and that the numbers $[q_1, q_2, q_3]$ represent a set of associated de-embedding parameters. The de-embedding function should provide an accurate prediction of T, based on the measured reflection Γ_m, but predicts a value $(T+\partial T)$.
The overview in figure 3 demonstrates that the de-embedding function can be transformed into a bilinear function, and thus that the relationship between measured value and de-embedded value has the following general form:

$$T + \partial T = \frac{q_1 - q_2 \cdot \Gamma_m}{1 - q_3 \cdot \Gamma_m}$$

$$q_1 - q_2 \cdot \Gamma_m + q_3 \cdot T \cdot \Gamma_m = T + \partial T \cdot (1 - q_3 \cdot \Gamma_m)$$

An optimal calibration requires that the average of absolute (∂T) or relative $(\partial T / T)$ errors, associated with the standard reflectors, is minimized in a least-squares sense.
Unfortunately, when a set of four or more simultaneous equations of this non-linear form has to be resolved in a least-squares sense, then the solution that minimizes the average error must be found in an iterative way.
A more convenient approach, that is superior in simplicity, will result in a slightly different solution close to this optimum. It is based on the optimization of a weighted error, of which the weighting factor is chosen to facilitate the linearization of the optimization equation.
We define the following concepts:

absolute error:	∂T
relative error:	$\partial T / T$
weighting factor:	$W = (1 - q_3 \cdot \Gamma_m)$
weighted error:	$W \cdot \partial T = (1 - q_3 \cdot \Gamma_m) \cdot \partial T$

This approach minimizes the weighted error instead of the absolute error, and is therefore called a *near-optimal* calibration. In some cases, the weighted error is close to the *absolute* error (∂T), and in other cases it is close to the *relative* error $(\partial T / T)$. This is worked out in section 3.
The use of a modified optimization goal, by the use of error weighting, will reduce the complexity of the equation to the following linear form:

$$q_1 - q_2 \cdot \Gamma_m + q_3 \cdot T \cdot \Gamma_m = T + W \cdot \partial T$$

Owing to this linear form, each calibration sample contributes to a row of the following matrix equation:

$$\begin{pmatrix} 1 & -\Gamma_{m1} & T_1.\Gamma_{m1} \\ 1 & -\Gamma_{m2} & T_2.\Gamma_{m2} \\ \vdots & \vdots & \vdots \end{pmatrix} * \begin{pmatrix} q_1 \\ q_2 \\ q_3 \end{pmatrix} = \begin{pmatrix} T_1 + W_1 \cdot \partial T_1 \\ T_2 + W_2 \cdot \partial T_2 \\ \vdots \end{pmatrix}$$

In the case of three standard reflectors, the solution for the de-embedding parameters is unique. When the absolute de-embedding error for these reflectors is defined as $\partial T=0$, then these parameters $[q_1, q_2, q_3]$ are found by matrix inversion followed by matrix multiplication. In the case of four or more reflectors, an exact solution, that fits all actual values T with zero error, does not exist in general.
A near-optimal solution minimizes the power average of the weighted errors $\langle |W_i \cdot \partial T_i|^2 \rangle$ in this overdetermined matrix equation. The least-squares solution of a set with linear equations is unique and can be found by an overdetermined left-hand matrix division. This is described in detail in section 4. Using the Matlab conventions for matrix division [5], the least-squares solution has the following closed mathematical form:

$$\begin{pmatrix} q_1 \\ q_2 \\ q_3 \end{pmatrix} = \begin{pmatrix} 1 & -\Gamma_{m1} & T_1.\Gamma_{m1} \\ 1 & -\Gamma_{m2} & T_2.\Gamma_{m2} \\ \vdots & \vdots & \vdots \end{pmatrix} \backslash \begin{pmatrix} T_1 \\ T_2 \\ \vdots \end{pmatrix}$$

When $[q_1, q_2, q_3]$ and $T(\Gamma_m)$ are substituted by the formulas summarized in figure 3, then the left-hand matrix division results in the near-optimal calibration solution for reflection, impedance and admittance. In figure 3, these solutions are tabulated.

near-optimal reflection calibration
that minimizes: $\langle |W_\Gamma \cdot \partial\Gamma|^2 \rangle \approx \langle |\partial\Gamma|^2 \rangle$

$$\begin{pmatrix} e_d/\Delta_E \\ 1/\Delta_E \\ e_s/\Delta_E \end{pmatrix} = \begin{pmatrix} 1 & -\Gamma_{m1} & \Gamma_1.\Gamma_{m1} \\ 1 & -\Gamma_{m2} & \Gamma_2.\Gamma_{m2} \\ \vdots & \vdots & \vdots \end{pmatrix} \backslash \begin{pmatrix} \Gamma_1 \\ \Gamma_2 \\ \vdots \end{pmatrix}$$

near-optimal impedance calibration
that minimizes: $\langle |W_Z \cdot \partial Z|^2 \rangle \approx \langle |\partial Z \cdot (1-\Gamma)|^2 \rangle$

$$\begin{pmatrix} (\Delta_E+e_d)/(\Delta_E-e_d) \\ (e_s+1)/(\Delta_E-e_d) \\ (e_s-1)/(\Delta_E-e_d) \end{pmatrix} = \begin{pmatrix} 1 & -\Gamma_{m1} & Z_1/Z_0.\Gamma_{m1} \\ 1 & -\Gamma_{m2} & Z_2/Z_0.\Gamma_{m2} \\ \vdots & \vdots & \vdots \end{pmatrix} \backslash \begin{pmatrix} Z_1/Z_0 \\ Z_2/Z_0 \\ \vdots \end{pmatrix}$$

near-optimal admittance calibration
that minimizes: $\langle |W_Y \cdot \partial Y|^2 \rangle \approx \langle |\partial Y \cdot (1+\Gamma)|^2 \rangle$

$$\begin{pmatrix} (\Delta_E-e_d)/(\Delta_E+e_d) \\ (e_s-1)/(\Delta_E+e_d) \\ (e_s+1)/(\Delta_E+e_d) \end{pmatrix} = \begin{pmatrix} 1 & -\Gamma_{m1} & Z_0/Z_1.\Gamma_{m1} \\ 1 & -\Gamma_{m2} & Z_0/Z_2.\Gamma_{m2} \\ \vdots & \vdots & \vdots \end{pmatrix} \backslash \begin{pmatrix} Z_0/Z_1 \\ Z_0/Z_2 \\ \vdots \end{pmatrix}$$

FIG 4 *An overview of near-optimal calibration solutions in closed mathematical form. The three requested de-embedding parameters $[e_d, \Delta_e, e_s]$ or $[e_d, e_r, e_s]$ can be obtained from the*

three elements of the solution vector by simple algebraic manipulations.

2.2 EXPERIMENTAL VERIFICATION

To demonstrate the improvement in accuracy, the data set that was measured in ref. [2] was used to compare a simple three-point calibration with the proposed robust multi-point calibration. The data set contained raw reflection measurement results on 14 offset Covers, 3 offset Opens and 2 offset Absorbers. The offset distance was varied in arbitrary steps from 0 to 2.5 m, and the frequency was varied in 55 logarithmic steps from 30 to 750 Hz.
Although an Open is not preferred as a *primary* calibration standard [2], all offset Opens were used as standard reflector in the robust calibration. The deviation from an ideal offset Open was modeled by an elongation of 22 mm of the offset tube, terminated with an ideal Open. All remaining errors are assumed to be within the measurement accuracy of the used Network Analyzer.

In theory, the de-embedded reflection magnitude of the Covers should have the value $|\Gamma_c|=1$, and of the Opens $|\Gamma_o|\approx 1$. In practical situations, a small deviation from the theoretical value will occur, caused by distortion and quantization in the Network Analyzer [2]. Figure 5 shows the magnitude of the de-embedded reflections with the simple three-point calibration that was described in ref. [2]. Figure 6 shows the de-embedded reflection magnitude of the same data set with robust near-optimal reflection calibration, based on all Covers and Opens.

The robust calibration has performed a significant improvement of the overall de-embedding accuracy over the full frequency range. In spite of more than 70% directivity (e_d), the method has even improved the de-embedding above 300 Hz. The absolute reflection error $\partial\Gamma$ of the de-embedded reflection from its theoretical value is shown in figure 7. The 1.5% rms averaged value of this error below 200 Hz is in agreement with the observed non-linear distortion in the Network Analyzer [2] and random effects caused by hum. For a few reflectors, this deviation was significantly higher than the rms-value, which is plotted as max-error.

Fig 5 *Reflection magnitude of various de-embedded offset Covers, Opens and Absorbers, in case a simple three-point calibration was performed with three offset Covers.*

Fig 6 *De-embedded reflection magnitude of the same data set that is used in figure 4, in case a robust near-optimal reflection calibration was performed with all offset Covers.*

Fig 7 *The deviation between de-embedded reflection and actual reflection, for all 14 Covers and 3 Opens. The rms-average of these errors is defined as* $\sqrt{\langle|\partial\Gamma|^2\rangle}$, *and the max error as* $|\partial\Gamma|_{max}$.

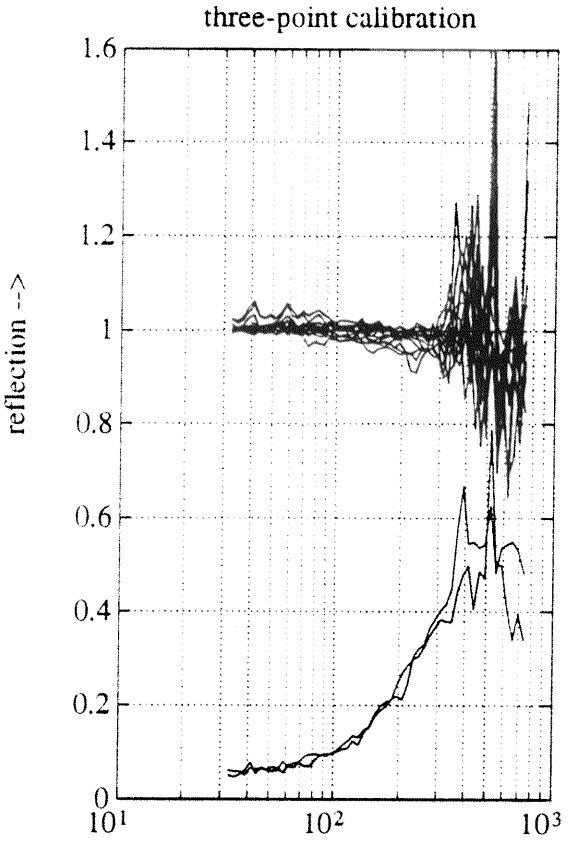


FIG 5. freq [Hz] -->

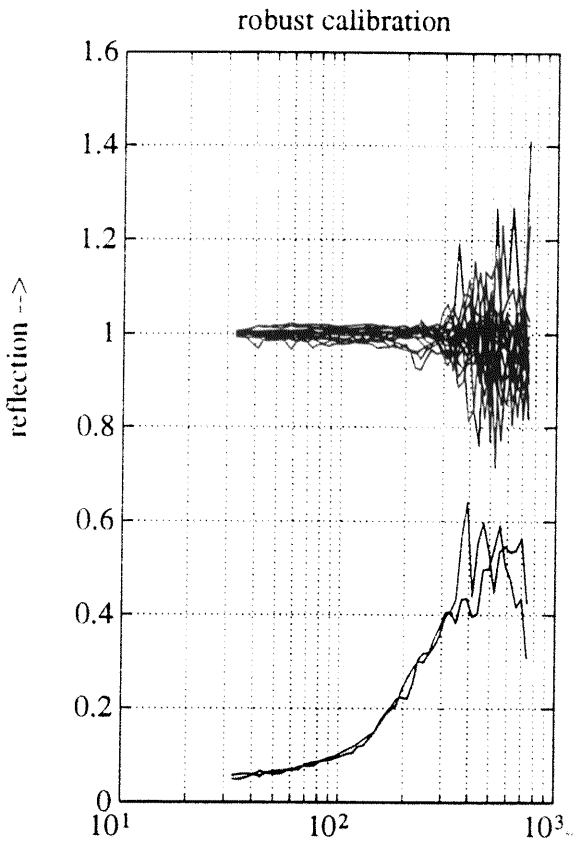


FIG 6. freq [Hz] -->

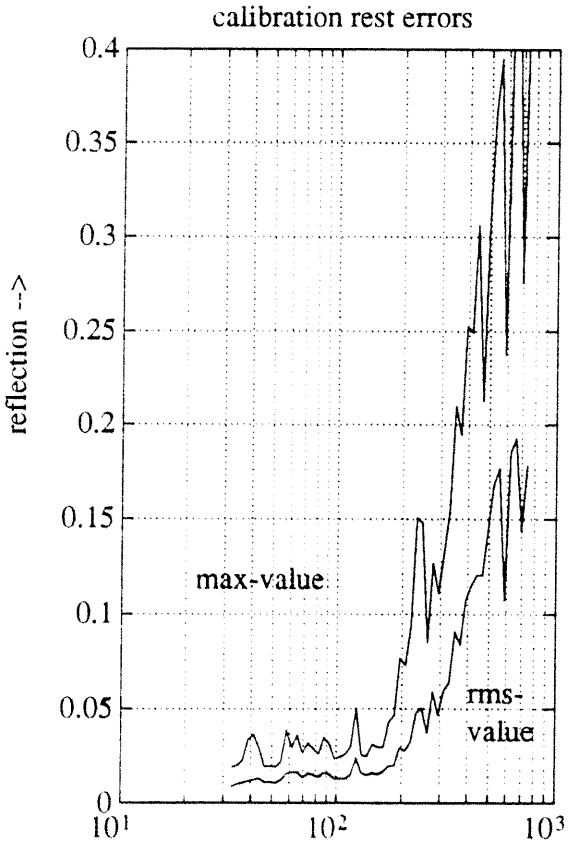


FIG 7. freq [Hz] -->

2.3 *INFINITE VALUE HANDLING FOR IMPEDANCE AND ADMITTANCE*

The formulae in figure 4 are not prepared for the substitution of infinite impedance or admittance values. In the limit $Z \rightarrow \infty$ or $Y \rightarrow \infty$ some matrix coefficients of the equation set will tend to infinity and cause the solution vector to be indefinite.
In practical situations, a standard reflector with infinite impedance or admittance is easy to construct. All offset Covers, located at positions such as 0, $\lambda/2$, λ, $3\lambda/2$ and offset Opens at positions such as $\lambda/4$, $3\lambda/4$, $5\lambda/4$ are associated with infinite impedance. The same applies for admittance when Opens and Covers have been switched.

One way to handle this problem is to exclude these standard reflectors from the calibration procedure, but this would require the exclusion of two of the most attractive standard reflectors: a Cover and an Open, located at the reference plane.
Fortunately, it is not required to substitute infinite numbers in the calibration equations, because the limited dynamic range of a practical network analyzer prevents the distinction of impedances above a well defined value, denoted as Z_{max}. Standard reflector values above this limit should therefore be clipped to Z_{max} before they are substituted in the calibration equations. The same applies for admittance de-embedding.
Assume that when $\Delta\Gamma$ is the quantization step of the used analog/digital converter, the reflection values between $(1-\Delta\Gamma)$ and (1) are indistinguishable. The associated upper impedance limit has therefore the value $Z_{max} = 2/\Delta\Gamma \cdot \mathbb{Z}_0$, which is equivalent to $Z_{max} = 256 \cdot \mathbb{Z}_0$ for an 8-bits A/D converter. For very high resolution A/D converters, this upper limit is merely caused by the system noise when its rms-value exceeds the quantization steps.

The previous approach is only applicable when the impedance accuracy of the standard reflector is preserved for high impedance values. This applies for Covers with zero offset, but not for $\lambda/2$ offset Covers or any multiple value. The uncertainty in sound velocity may then dominate the reflection phase error, and thus the impedance uncertainty.
The resonating peaks in the impedance versus frequency plots suffer from reduced accuracy, compared to the impedance accuracy of values close to $\mathbb{Z}_0$. Therefore it is sensible to exclude all samples in the calibration equations of which the uncertainty exceeds a predefined value. This exclusion process is highly frequency selective: the smaller the wavelength λ, the more the usable impedance range is reduced.
The calculation of the usable impedance range of an offset reflector at distance x is worked out in section 3.5. In the experiments that are described here, all impedance values are excluded from calibration that meets $|Z/\mathbb{Z}_0| > 10 \cdot \lambda/x$. The same applies for $|Y \cdot \mathbb{Z}_0| > 10 \cdot \lambda/x$.

3. ACCURACY OF THE DE-EMBEDDING

The overall accuracy is limited by the accuracy of the standard reflectors, by uncertainties caused by random effects such as drift, noise and hum, and by non-linear effects in the Network Analyzer. In general, the term *"accuracy"* is not unambiguous and has to be well defined.

In this section, we first specify which accuracy error terms are analyzed, and we draw a distinction between balanced and unbalanced accuracy errors. Then, the relationship between absolute and weighted calibration errors is evaluated for the three calibration methods. The associated weighting factor is used to analyze the unbalance in de-embedding accuracy for all described

calibration methods. Next, this analysis is used to specify which calibration method is preferred in which situation. Further, the accuracy of offset reflectors is analyzed, to specify when reflection values should be excluded from the calibration. Finally, the conclusions from these accuracy unbalance calculations are verified experimentally by means of impedance de-embedding.

3.1 BALANCED AND UNBALANCED ACCURACY

A definition that is useful for *accuracy error is* application-dependent. In the special case that the ratio between absorbed and available acoustic power is measured, the absolute reflection error $\partial\Gamma$ is commonly appropriate to describe the measurement accuracy. As demonstrated in section 3.2, this absolute reflection error is roughly proportional with the relative impedance error $\partial Z/Z$ or with $\partial Y/Y$. For this reason, we have confined ourselves in this section to the optimization of the accuracy error terms: $\partial\Gamma$, $\partial Z/Z$ and $\partial Y/Y$.

An optimal calibration method extracts a set of de-embedding parameters by which all accuracy errors are uniformly spread out over the full measurement range. This is called *"balanced accuracy"*.
When a near-optimal calibration is performed, the resulting de-embedding accuracy may not be balanced. For instance, when a near optimal impedance calibration is performed for impedance de-embedding, then the relative impedance accuracy is highly unbalanced for low impedance values. In section 3.3 it is demonstrated that the relative accuracy is in this case improved for high impedance value, at the cost of a decreased accuracy for low values. This is the disadvantage of the performed simplification of the calibration equations, by means of error weighting. In the next sections, the unbalance inaccuracy is analyzed.

3.2 ERROR WEIGHTING FACTORS

When the actual quantities Γ, Z or Y are de-embedded from the measured reflection Γ_m, then the absolute error is denoted with $\partial\Gamma$, ∂Z or ∂Y. The general relationship between weighted error and absolute error is defined in section 2.1 by: $W\cdot\partial T = \partial T\cdot(1-q_3\cdot\Gamma_m)$. When the acoustic network analyzer is well engineered, then this expression can be simplified and reduces by approximation to:

$$\left\{\begin{array}{l} |\Delta_E| \approx 1 \\ |e_d| \ll 1 \\ |e_s| \ll 1 \end{array}\right\} \Longrightarrow \quad \Gamma \approx (-1/\Delta_E)\cdot\Gamma_m$$

$$\begin{aligned} W_\Gamma\cdot\partial\Gamma &= \partial\Gamma\cdot(1-(e_s/\Delta_E)\cdot\Gamma_m) &&\approx \partial\Gamma \\ W_Z\cdot\partial Z &= \partial Z\cdot(1-(e_s-1)/(\Delta_E-e_d)\cdot\Gamma_m) &&\approx \partial Z\cdot(1-\Gamma) \\ W_Y\cdot\partial Y &= \partial Y\cdot(1-(e_s+1)/(\Delta_E+e_d)\cdot\Gamma_m) &&\approx \partial Y\cdot(1+\Gamma) \end{aligned}$$

Because Γ, Z and Y are mutually related, their absolute errors $\partial\Gamma$, ∂Z and ∂Y are also mutually related. The required accuracy equation, is derived from the following expression:

$$\frac{1+\Gamma}{1-\Gamma} = Z/Z_0 = 1/YZ_0$$

The logarithm results in

$$\ln(1+\Gamma)-\ln(1-\Gamma) = \ln(Z) - \ln(Z_0) = -\ln(Y) - \ln(Z_0)$$

and the derivation leads to

$$\frac{2\cdot\partial\Gamma}{(1+\Gamma)\cdot(1-\Gamma)} = (\partial Z/Z) = -(\partial Y/Y)$$

This expression demonstrates that for reflection values below 70%, the defined accuracy error terms are roughly proportional. Based on the above relationship between accuracy errors and the approximated weighted error, the relationships between the (balanced) weighted errors and the (unbalanced) accuracy errors are calculated. Figure 8 tabulates these relationships for various calibration methods.

		Γ	Z	Y
near-optimal reflection calibration	$\frac{\lvert W\cdot\partial\Gamma\rvert}{2}$	$\left\lvert\frac{\partial\Gamma}{2}\right\rvert$	$\left\lvert\frac{\partial Z/Z}{Z/\mathbb{Z}_0+2+\mathbb{Z}_0/Z}\right\rvert$	$\left\lvert\frac{\partial Y/Y}{Y\mathbb{Z}_0+2+1/Y\mathbb{Z}_0}\right\rvert$
near-optimal reflection calibration	$\frac{\lvert W\cdot\partial Z\rvert}{2}$	$\left\lvert\frac{\partial\Gamma}{1-\Gamma}\right\rvert$	$\left\lvert\frac{\partial Z/Z}{1+\mathbb{Z}_0/Z}\right\rvert$	$\left\lvert\frac{\partial Y/Y}{1+Y\mathbb{Z}_0}\right\rvert$
near-optimal reflection calibration	$\frac{\lvert W\cdot\partial Y\rvert}{2}$	$\left\lvert\frac{\partial\Gamma}{1+\Gamma}\right\rvert$	$\left\lvert\frac{\partial Z/Z}{1+Z/\mathbb{Z}_0}\right\rvert$	$\left\lvert\frac{\partial Y/Y}{1+1/Y\mathbb{Z}_0}\right\rvert$

Fig 8 *Approximated relationship between the balanced weighted errors and the unbalance accuracy errors, in a well engineered acoustic network analyzer. The near-optimal calibration has optimized the weighted error in a least-squares sense. This means that the power average* $\langle|W\cdot\partial\Gamma|^2\rangle$, $\langle|W\cdot\partial Z|^2\rangle$ *or* $\langle|W\cdot\partial Y|^2\rangle$ *is minimized.*

3.3 ANALYSIS OF UNBALANCE IN DE-EMBEDDING ACCURACY

The weighting factor W was introduced in section 2.1 to linearize the overdetermined equations for simplification purposes. As a consequence, the average *weighted* error $\langle|W\cdot\partial T|^2\rangle$ was minimized instead of the average absolute error$\langle|\partial T|^2\rangle$.
The weighting function $\mathcal{W}$ relates the weighted error $W\cdot\partial T$ with the accuracy error. In the case that the absolute error ∂T is defined as accuracy error, weighting function and weighting factor are equal, but in the case that the relative error $\partial T/T$ was used as accuracy error, then $\mathcal{W} = W\cdot T$ holds.

If the weighting function is a constant for all accuracy errors, then the weighting has no effect on the solution. All accuracy errors are then equally minimized and thus perfectly balanced over the full de-embedding range.
If the weighting function varies with the de-embedding value, then its average value is still irrelevant, but the deviation from this average affects the resolved de-embedding parameters. The higher the weighting, the more an individual calibration error is pronounced in the average of the weighted error, and the more the error will dominate in the minimization algorithm. If small errors in privileged ranges are as important as large errors in disadvantaged ranges, then the resolved de-embedding parameters facilitate an increased de-embedding accuracy in the privileged ranges at the cost of an accuracy decrement in disadvantaged ranges. This effect causes the accuracy unbalance.

As a rule of thumb, the accuracy unbalance is proportional to the magnitude of the weighting function. The highest accuracy will be observed in the privileged ranges, associated with the highest weighting. Because this statement holds only exactly in situations where all values of the selected standard reflectors are equally spread out over the de-embedding range, the unbalance in weighting function is merely indicative of the unbalance in de-embedding accuracy.

Figure 9 shows the magnitude of the weighting functions in a graphic way, based on the formulae of figure 8. Because their average value is irrelevant, the weighting curves are normalized with respect to the maximum value. The privileged ranges, in which the weighting exceeds the threshold of half the maximum value, are emphasized in the plots of figure 9. Within these ranges the de-embedding accuracy is assumed to be maximal.

Fig 9: *Graphic illustration of the normalized weighting function, which is indicative of the unbalance in de-embedding accuracy. The emphasized curves demarcate the privileged ranges in which the accuracy is maximal. The (o) marker marks the values for* $\Gamma=0$, $Z=\mathbb{Z}_0$ *or* $Y=1/\mathbb{Z}_0$.
The weights for the special case of impedance calibration, intended for reflection de-embedding, tends to infinity for $\Gamma\rightarrow 1$ *which forces the normalized weighting function to zero for all* $\Gamma\neq 1$. *The same applies for admittance calibration.*

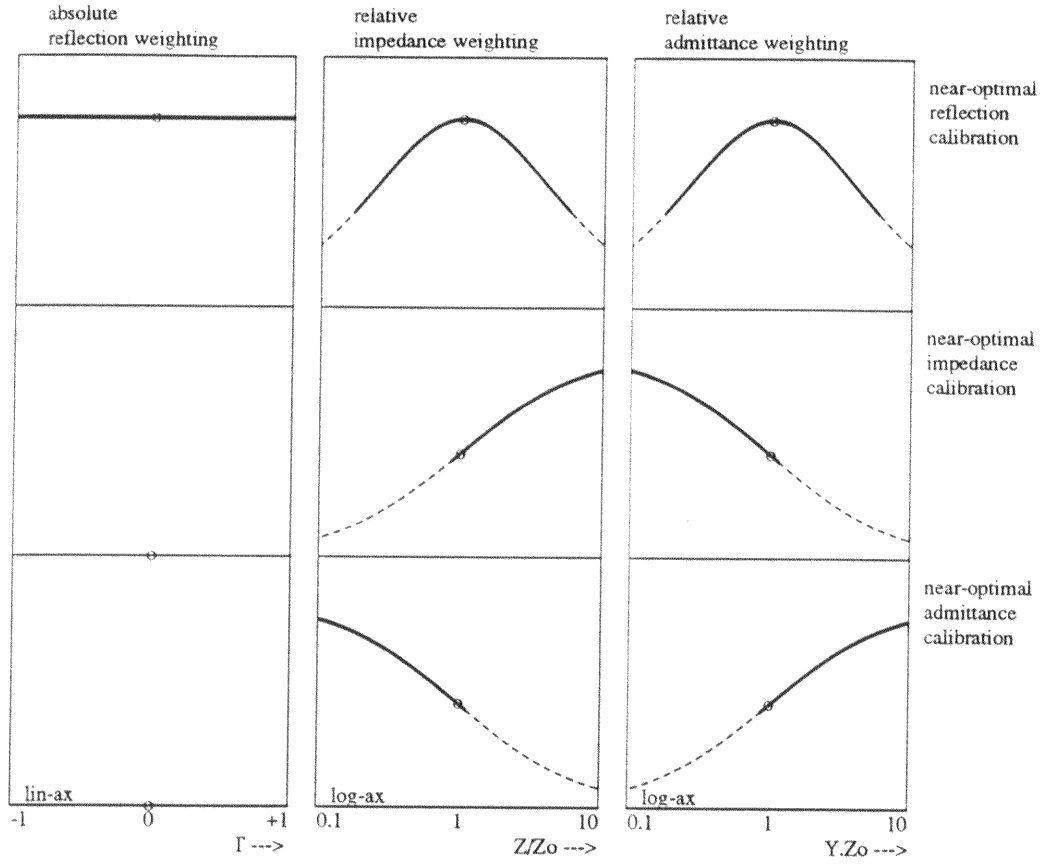

absolute
reflection weighting
relative
impedance weighting
relative
admittance weighting
near-optimal
reflection
calibration
near-optimal
impedance
calibration
near-optimal
admittance
calibration
lin-ax
log-ax
log-ax
-1
0
+1
Γ --->
0.1
1
10
Z/Zo --->
0.1
1
10
Y.Zo --->

FIG 9

3.4 *THE PREFERRED CALIBRATION METHOD*

The plots in figure 9 demonstrate that the privileged de-embedding range is closely related to the type of de-embedding and to the used calibration method. Balanced accuracy is only available for reflection de-embedding.
For impedance and admittance de-embedding, the accuracy unbalance restricts the usable de-embedding range to a privileged and a neutral range. Fortunately, these ranges are complementary for impedance an admittance calibration, and are overlapped by the privileged range of reflection calibration. This facilitates a choice for a specific calibration method based on the de-embedding range of interest. Figure 10 tabulates the preferred method for various situations.

error	*prefered calibration method*
$\partial\Gamma$	use always near-optimal reflection calibration
$\frac{\partial Z}{Z}$	$Z \gg \mathbb{Z}_0 \longrightarrow$ near-optimal impedance calibration $Z \approx \mathbb{Z}_0 \longrightarrow$ near-optimal reflection calibration $Z \ll \mathbb{Z}_0 \longrightarrow$ near-optimal admittance calibration
$\frac{\partial Y}{Y}$	$Y \gg 1/\mathbb{Z}_0 \longrightarrow$ near-optimal admittance calibration $Y \approx 1/\mathbb{Z}_0 \longrightarrow$ near-optimal reflection calibration $Y \ll 1/\mathbb{Z}_0 \longrightarrow$ near-optimal impedance calibration

Fig 10 The preferred calibration method, for various de-embedding ranges of interest.

It is unlikely to de-embed values in the disadvantaged accuracy ranges. Reversely, when a standard reflector is used for the calibration, and its value is within an disadvantaged accuracy range, then the associated weighting reduces the sensitivity of the de-embedding parameter-extraction to variations of the standard reflection value. Below 10% error weighting, only the strongest variations will be noticed in the calibration procedure. Therefore, as a rule of thumb, the addition of an extra standard reflector to the calibration, will not improve the overall calibration accuracy when its normalized weighting is below 10%.

3.5 *ACCURACY LIMITS OF STANDARD REFLECTORS*

The overall de-embedding accuracy of the Network Analyzer is restricted by random and non-linear instrument errors, and by the accuracy limits of the standard reflectors. The inaccuracy in sound velocity causes that the reflection phase error increases with the frequency, and that in special situation all measurement errors are dominated by phase errors of the standard reflectors.
Assume that c is the sound velocity, that the offset length of the reflector is x, and that $\lambda=2\pi f/c$ is the wavelength in the tube. Then the offset reflection Γ is related as follows to the reflection Γ_o at zero offset:

$$\Gamma = e^{-j\cdot 2x/\lambda}\cdot\Gamma_o = e^{-j\cdot 2x\cdot 2\pi f/c}\cdot\Gamma_o$$

A small variation of ∂c in sound velocity causes a small variation in the value of the standard reflector, and reduces the accuracy of the standard. Under the condition that all other physical quantities remain preserved, the accuracy errors are proportional with the relative accuracy of the sound velocity. This proportionality is represented by accuracy reduction factors η, which are defined as follows:

$$\eta_\Gamma \equiv \left|\partial\Gamma\right| / \left|\frac{\partial c}{c}\right| = c \cdot \left|\frac{\partial\Gamma}{\partial c}\right| = \left(\frac{x}{\lambda}\right) \cdot \left|2 \cdot \Gamma\right|$$

$$\eta_Z \equiv \left|\frac{\partial Z}{Z}\right| / \left|\frac{\partial c}{c}\right| = \frac{c}{Z} \cdot \left|\frac{\partial Z}{\partial c}\right| = \left(\frac{x}{\lambda}\right) \cdot \left|\mathbb{Z}_0/Z - Z/\mathbb{Z}_0\right|$$

$$\eta_Y \equiv \left|\frac{\partial Y}{Y}\right| / \left|\frac{\partial c}{c}\right| = \frac{c}{Y} \cdot \left|\frac{\partial Y}{\partial c}\right| = \left(\frac{x}{\lambda}\right) \cdot \left|(\mathbb{Z}_0 \cdot Y) - 1/(\mathbb{Z}_0 \cdot Y)\right|$$

These equations demonstrate that the accuracy errors are affected by the actual reflection value. This effect is of minor importance for the reflection value, but can dramatically decrease the accuracy for high and low impedance and admittance values.
The accuracy reduction factor η is useful to specify whether the inaccuracy of a standard reflector exceeds a predefined value or not. For instance, in a practical situation of ±1 m/s uncertainty in sound velocity, which is equivalent to 0.3% inaccuracy, and a chosen inaccuracy limit of 3%, all reflectors of which the accuracy reduction factor η exceeds the value η=10 must be excluded from the calibration procedure.

In figure 11, the interval limits of the usable standard reflector values are tabulated in the case that the offset phase errors are dominating. Between these limits, the accuracy errors as defined in section 3.1 remains below a predefined upper limit, specified by η. Standard reflector values outside this interval must be skipped, because their inaccuracy is too high. The same applies for admittance calibration and low admittance values.
Figure 12 demonstrates the impedance accuracy range for an offset Cover.

standard value	*accuracy error*	*lower limit*	*upper limit*	*remarks*
$\left\|\Gamma\right\|$	∂Z	0	$\left(\frac{\lambda\eta}{2x}\right)$	*when* Γ_0 *is frequency independent, then* $\left(\frac{x}{\lambda}\right) = \frac{f}{2\Gamma} \cdot \left\|\frac{\partial\Gamma}{\partial f}\right\|$
$\left\|Z/\mathbb{Z}_0\right\|$	$\frac{\partial Z}{Z}$	$\left(\frac{x}{\lambda\eta}\right)$	$\left(\frac{\lambda\eta}{x}\right)$	
$\left\|Y \cdot \mathbb{Z}_0\right\|$	$\frac{\partial Y}{Y}$	$\left(\frac{x}{\lambda\eta}\right)$	$\left(\frac{\lambda\eta}{x}\right)$	

Fig 11 Lower and upper limits for the values of a standard reflector, to prevent the offset phase error from exceeding a predefined value. To preserve the specified accuracy, all standard reflector values outside these ranges must be skipped. For near-optimal calibrations, the lower limits may be ignored.

Fig 12 Accuracy range of the impedance of an offset Cover, with 1 m offset distance, in the case that the accuracy reduction factor is limited to a chosen value η_Z*=10.*

In the case that a near-optimal impedance calibration is performed, the error weighting causes the calibration to be insensitive to large errors associated with low impedance values. Skipping of low impedance standard reflectors will not affect the overall calibration accuracy, and therefore the lower limits in figure 11 may be ignored for near-optimal calibration.

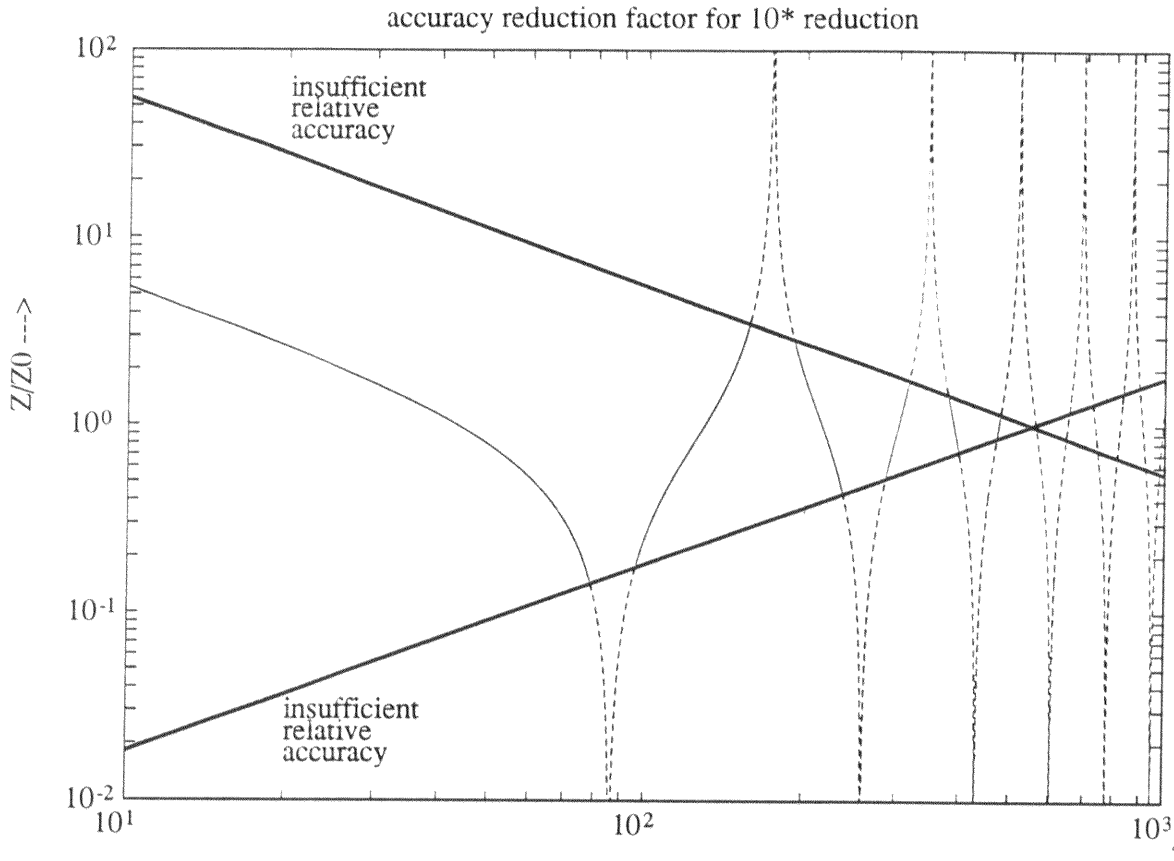


FIG 12 freq [Hz] --->

3.6 EXPERIMENTAL VERIFICATION OF ACCURACY RANGES

To verify the conclusions, tabulated in figure 10, a set of six offset Covers and six offset Opens, ranging from 0 to 0.35 [m] was measured. The frequency was varied in 44 logarithmic steps from 30 to 400 Hz. Then, the de-embedding parameters were extracted by all three robust calibration methods, using all twelve reflectors. Finally, the impedance was de-embedded and compared with the specified actual values of the standard reflectors. The figures 13 to 15 show all results.

In these plots all high impedance and admittance values, associated with an accuracy reduction factor η above η=10, are ignored during the calibration. The privileged and neutral accuracy ranges, predicted by the unbalance accuracy considerations of section 3.4, are marked in these figures with vertical bars. These bars are limited by the quantization boundaries described in section 2.3. The shape of the impedance curves within the predicted accuracy ranges are significantly smoother than beyond these range limits. This validates the conclusions tabulated in fig 10.

Fig 13 *Comparison of the de-embedded impedance (solid lines) and the actual impedance (dotted lines), in case a near-optimal impedance calibration is performed. The position of the vertical bar indicates the optimal accuracy range for high impedance values.*

Fig 14 *Comparison of the de-embedded impedance (solid lines) and the actual impedance (dotted lines), in case a near-optimal admittance calibration is performed. The position of the vertical bar indicates the optimal accuracy range for low impedance values.*

Fig 15 *Comparison of the de-embedded impedance (solid lines) and the actual impedance (dotted lines), in case a near-optimal reflection calibration is performed. The position of the vertical bar indicates the optimal accuracy range for medium impedance values.*

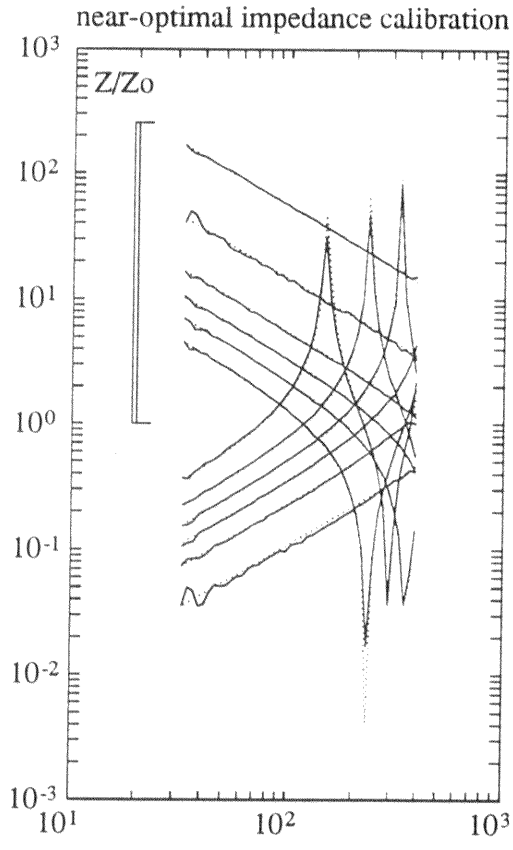


FIG 13 freq [Hz] -->

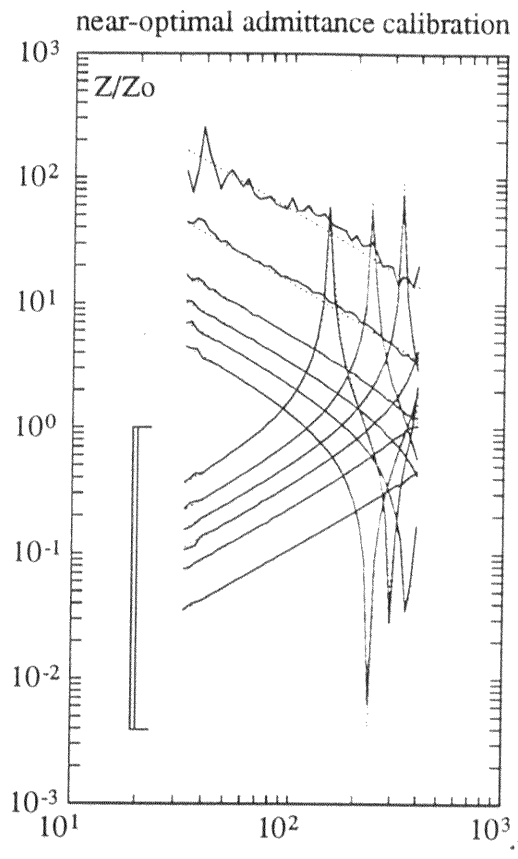


FIG 14 freq [Hz] -->

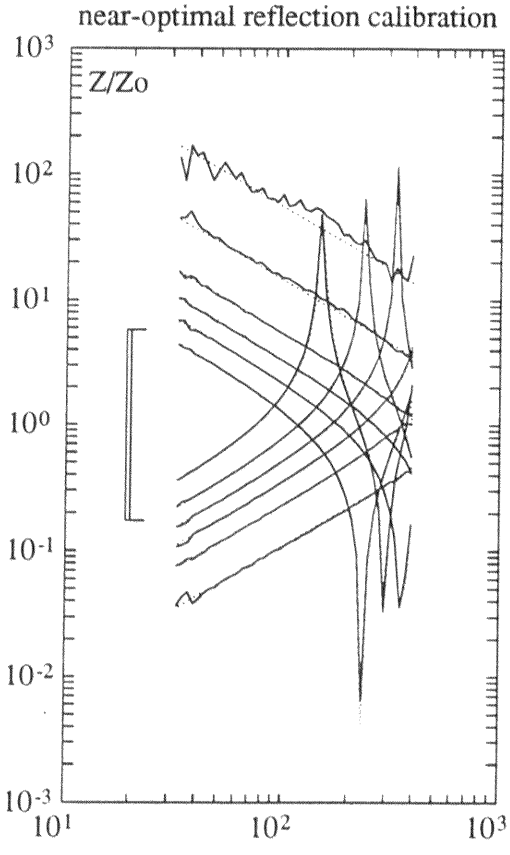


FIG 15 freq [Hz] -->

4. ALGORITHMS FOR OVERDETERMINED EQUATIONS

In section 2.1, an equation set for three variables was resolved for the case that four or more equations were available. In general, there exists no exact solution and therefore a fair solution was used that minimizes all errors in a least-squares sense. This section describes the algorithms that are required for the evaluation of this least-squares solution.

4.1. DEFINITIONS

The least-squares solution of an overdetermined set of linear equations, represented by the matrix equation $A \cdot x \approx b$, is denoted with a vector x. By definition, this solution vector x minimizes the deviation $(A \cdot x - b)$ in a least-squares sense. Either the (m*n) matrix A, as the (m*1) column vector b, as the (n*1) column vector x, may contain complex numbers.
If A is an invertible square matrix, then an exact solution is formed by the matrix expression $x = A^{-1} \cdot b$, but in general ($m \geq n$) a left hand matrix division is required. For any rectangular (m*n) matrix A, of which the square (n*n) matrix $(A' \cdot A)$ is invertible, the matrix division is defined as follows:

$$\left.\begin{aligned} A \backslash b &\equiv (A' \cdot A)^{-1} \cdot (A' \cdot b) \\ A' &= \mathrm{conj}(A^{T}) \end{aligned}\right\}$$

In this definition, the generalized transpose A' is used, instead of the element wise transpose A^{T}. The generalized transpose swaps *and* conjugates the elements, to facilitate that $(b' \cdot b)$ remains a positive real number when the elements of b are complex.

4.2. LEAST-SQUARES SOLUTION

The column vector A\b forms a fair solution for $A \cdot x \approx b$ and is, as follows, associated with a small deviation vector Δb:

$$\left.\begin{aligned} A \cdot x &= b + \Delta b \\ x = A \backslash b &= (A' \cdot A)^{-1} \cdot (A' \cdot b) \end{aligned}\right\}$$

To prove that this solution x minimizes $|\Delta b|^2 = \Delta b' \cdot \Delta b$ in a least-squares sense, another solution vector $x+\Delta x$ is considered. The associated deviation suits:

$$\left.\begin{aligned} A \cdot (x+\Delta x) &= b + \Delta b + A \cdot \Delta x \\ (A' \cdot A) \cdot x &= A' \cdot b \end{aligned}\right\}$$

$$\left.\begin{aligned} A \cdot (x+\Delta x) &= b + \Delta b + A \cdot \Delta x \\ A' \cdot (A \cdot x - b) &= A' \cdot \Delta b = 0 \end{aligned}\right\}$$

The associated deviation $(\Delta b + A \cdot \Delta x)$ is related to (Δb) as follows:

$$|\Delta b + A \cdot \Delta x|^2 = \Delta b' \cdot \Delta b + (A \cdot \Delta x)' \cdot (A \cdot \Delta x) + \Delta b' \cdot (A \cdot \Delta x) + (A \cdot \Delta x)' \cdot \Delta b$$

$$|\Delta b + A \cdot \Delta x|^2 = |\Delta b|^2 + |A \cdot \Delta x|^2 + 2 \cdot (\Delta x' \cdot A' \cdot \Delta b)$$

$$|\Delta b + A \cdot \Delta x|^2 = |\Delta b|^2 + |A \cdot \Delta x|^2$$

$$|\Delta b + A \cdot \Delta x|^2 \geq |\Delta b|^2$$

This proves that for all non-zero Δx, the deviation associated with $(x+\Delta x)$ is higher than the deviation associated with (x), and therefore $x = A \backslash b$ must be a unique least-squares solution.

4.3. ALGORITHM

Although the definition of the matrix division has facilitated a direct evaluation, a more appropriate approach is recommended. In the special case that A is square, the evaluation of the matrix division reduces to a straight forward matrix inversion:

$$\begin{aligned} A\backslash b &= (A'\cdot A)^{-1}\cdot(A'\cdot b) \\ &= (A)^{-1}(A')^{-1}\cdot(A')\cdot b \\ &= A^{-1}\cdot b \end{aligned}$$

In the general case that A is rectangular, the definition is reduced by means of the QR decomposition of matrix A in an orthogonal matrix Q and an upper triangle matrix R. Because $A = Q\cdot R$ and $Q'\cdot Q = I$ by definition, the evaluation of the matrix division reduces to:

$$\begin{aligned} A\backslash b &= (R'\cdot Q' \cdot Q\cdot R)^{-1}\cdot(R'\cdot Q'\cdot b) \\ &= (R'\cdot R)^{-1}\cdot(R'\cdot Q')\cdot b \\ &= R \setminus (Q'\cdot b) \end{aligned}$$

The benefit of this approach is that the upper triangle form of R dramatically simplifies the division, because many elements are zero. If back substitution ([4], section 2.2) is performed, then an explicit division with R is not required. Further, a robust QR-factorization, based on Householder transformations ([4], section 11.2) reduces numerical round-off errors for ill-conditioned matrices A. And finally, the explicit evaluation of Q is not required if each Householder transformation step, that reduces A toward R, is simultaneously performed on vector b.

5. CONCLUSIONS

A robust calibration method is proposed for acoustic Network Analyzers equipped with full error correction. It has been demonstrated that the de-embedding accuracy is improved, and that the method is insensitive to random calibration errors.
The improvement has been achieved by addition of redundancy to the calibration procedure, using a large number of standard reflectors. A set with many reflectors facilitates the errors to be equally spread out over all individual calibration measurements.
The accuracy improvement of the proposed method has been verified experimentally, and is compared with the accuracy of a simple three point calibration.

A robust calibration, optimized for reflection de-embedding, is associated with large accuracy errors for impedance or admittance de-embedding, in the case their values goes to zero or infinity. This restricts the applicability of the instrument. The functionality of the instrument is extended with impedance and admittance measurements, by the development of additional calibration methods optimized for impedance de-embedding or optimized for admittance de-embedding. These methods can even handle infinite values for impedance or admittance.

A near-optimal calibration method is developed, to linearize the calibration equations. As a result, the use of iterative calculation methods has been avoided, and all calibration equations have been resolved in closed mathematical form.

A detailed error analysis has demonstrated that the absolute accuracy degradation of a near-optimal reflection calibration, compared to a fully optimized calibration, is negligible. In the case of near-optimal impedance calibration, the degradation of relative de-embedding accuracy is restricted to small impedance values only. The validation of this error analysis is demonstrated by experiments.

6. REFERENCES

[1] C.M. de Blok and R.F.M. van den Brink, *"A direct reading one-port Acoustic Network Analyzer"*, submitted (july 1992) and accepted (jan 1993) for publication, in J. Audio Eng Soc.

[2] R.F.M. van den Brink and C.M. de Blok, *"A One-Port Acoustic Network Analyzer with full error correction"*, submitted (sept 1992) for publication, in J. Audio Eng Soc.

[3] C.M. de Blok and R.F.M. van den Brink, *"Full Characterization of linear acoustic networks based on N-ports and S-parameters"*, J. Audio Eng Soc, vol 40, pp517-523, (june 1992).

[4] W.H. Press et. al., *"Numerical recipes in Pascal"*, Cambridge 1989, Cambridge University Press.

[5] C. Moler et.al, *"PRO-Matlab User's guide"*, june 1989, The Mathworks Inc. USA.

7. THE AUTHORS

R.F.M. (Rob) van den Brink was born 1955, May 21. He graduated in 1984 from the Technical University Delft in the Netherlands, with a degree in electrical engineering. His graduation project concerned the development of feeds for microwave antennas. He joined the same university to work on microwave remote sensing experiments, but changed in 1985 to join PTT Research in the Netherlands.
Since then he worked on fiber-optical transmission systems. He developed wide band optical receivers and transmitters up to a few GHz, and various new measurement and software design tools for opto-electronic circuits. His group designed various analog circuits for coherent optical transmission systems, both for internal projects as for an ESPRIT (UCOL) project supported by the EEC.
Currently he is working on his PhD-theses on a systematic design approach for wide band analog circuits, applied to high performance optical receivers. He is author and coauthor of publications on optical receivers, noise measurements with lightwave components and acoustic network analysis, and of two patents (pending) on lightwave noise measurement and a lightwave noise source.

C.M. (Kees) de Blok was born on 1954, July 6. After an electrotechnical education he joined PTT Research in August of 1971. There he worked in different telecommunication areas such as audio/video transmission, scribofonie, and digital filters, until 1978.
He then became involved with the development of measuring installation methods for the first direct detection optical fiber links in the Netherlands. In this field he gained two patents: one for an optical directional coupler and another for a fiber alignment system. He was also coauthor of a publication on fiber installation. Since 1984 he has worked on the development and realization of different coherent optical links and has been co-author of a few conference proceedings on distribution and subscriber networks.
In addition to his work at PTT-research, in 1985 he started research on thermo-acoustic energy conversion. He si now working with others on modeling the complete thermo-acoustic process.